STRAIN HARDENING AND STRAIN RATE CHARACTERISTICS OF UNIAXIAL COLD COMPACTED SALT POWDERS

Mahir H. H. Es-Saheb

Mechanical Engineering Department, College of Engineering
King Saud University
P.O. Box 800, Riyadh 1142, Saudi Arabia

الخلاصـة :

تَـمَّ بحث تأثير التَّـصلب بالانفعال ، وكذا معدل الانفعال (التوتر) في الدمج (الـدَّك) على البارد لمجموعة متنوعة من مساحيق الأملاح وذلك باستخدام سلسلة من إختبارات الدمج الديناميكي أحادي المحور . وقد تمت تغطية مدى معدل انفعال من ١٠$^{-٣}$ إلى ١٠^{٥} لكلِّ ثانية لمساحيق كلوريد الصوديوم (ملح الطعام) وبروميد البوتاسيوم وفوسفات الكالسيوم وكبريتات النحاس . وَقُـيِّـمـت هذه المواد جميعها باستخدام الثوابت المشتقة من قانون القوىٰ والمعطىٰ كالتالي :

$$\sigma = B\ \varepsilon^{n}\ \dot{\varepsilon}^{m}$$

حيث أن σ تمثل الإجهاد المحوري (الضغط) عند انفعال ε ومعدل انفعال $\dot{\varepsilon}$ و n هو أُس التصلب بالانفعال و m أُس حساسية معدل الانفعال و B ثابت .

أظهر البحث أنه كلما زادت قِيم مُعدلات الانفعال فإنَّ أُس التصلب بالإنفعال n ، وأس معدل الانفعال m ، وجهد الإنسياب ، ومعامل القوة E جميعها - تزداد بصورة لاخطية لكافة المواد المُـخْـتَـبـرة . وتُـعـزىٰ هذه التفاوتات إلى التغير إما من السلوك اللدن إلى التقصفي أو الإنخفاض في كمية التشوه اللدن بسبب طبيعة اعتماد إجهاد الانسياب على الزمن . ويمكن تفسير هذه النتائج عن طريق أساليب الإنخلاع أو الانتشار المسؤولة عن آلية التشوه اللدن خلال أسلوب الدمج . فعند السرعات البطيئة تكون آلية الانخلاع هي المسيطرة وماتلبث أن تُستبدل بصيغة ما من أسلوب الانتشار عند السرعات (المعدلات) العالية . فقد وُجد ، للمواد التي تم اختبارها أنَّ كبريتات النحاس البلورية التقصفية هي الأكثر تصلباً بالانفعال ، والأقل حساسية لمعدلات الانفعال على عكس بروميد البوتاسيوم ، (الذي وُجد بأنه الأقل تصلباً بالانفعال والأكثر حساسية لمعدلات الانفعال) .

ABSTRACT

The influence of strain hardening and strain rate on the cold compaction of a variety of salt powders is investigated in a series of dynamic uniaxial compression tests. Strain rate range of 10^{-3} to 10^{5} s^{-1} is covered for sodium chloride, potassium bromide, calcium phosphate, and copper sulfate powders. These materials have been assessed using the constants derived from the power law given as:

$$\sigma = B\varepsilon^{n}\dot{\varepsilon}^{m}$$

where σ is the axial stress (pressure) at the induced strain ε, $\dot{\varepsilon}$ the strain rate, n the strain hardening exponent, m the strain rate sensitivity exponent, and B a constant.

The investigation show that as the strain rate increases the values of the strain hardening exponent n, the strain rate exponent m, the flow stress and the strength coefficient E are increased in a non-linear manner for all materials tested. These variations are attributed to a change either from ductile to brittle behavior or a reduction in the amount of plastic deformation due to the time dependent nature of the plastic flow. This, however, is explained in terms of dislocation and diffusion processes responsible for plastic deformation mechanisms during the compaction process. At low speeds the dislocation mechanisms are dominant, soon replaced by some form of diffusion process at higher speeds (rates). For the materials tested, the brittle crystalline copper sulfate is found to be the most strain hardening and the least strain rate sensitive material, while potassium bromide is found to be the reverse (*i.e.* the least strain hardening and the most strain rate sensitive material).

STRAIN HARDENING AND STRAIN RATE CHARACTERISTICS OF UNIAXIAL COLD COMPACTED SALT POWDERS

INTRODUCTION

In the early 1800s, in the field now known as powder metallurgy, the first published description of powder compaction is encountered. In 1829 Wallaston [1] described his development of a toggle press for the production of aluminum from aluminum powder. However, serious attempts at studying the relation between applied pressure and material deformation were not made until the 1920s. Among these are, the early works carried out by Shaxby and Evans [2] and by Walker [3]. The proposition of an equation relating applied pressure to the volume change of a powder compact by Jones [4] and a different but similar equation by Balshin [5] made a considerable impact on the study of powder compaction. The search was on for the best relationship that will describe the compaction process. There were several equations proposed but it was notable that Konopicky [6], Shapiro [7], and Heckel [8] arrived at a fairly similar constitutive equation using different assumptions. Now generally known as the Heckel equation, and given as:

$$\ln[1/(1-D)] = KP + A \tag{1}$$

it implies a linear relationship between pressure P and $\ln[1/(1-D)]$, where D is the relative density, K is a constant the reciprocal of which is equal to the mean yield pressure of the powder, and A is a constant. This equation and a rival one put forward by Kwakita [9] become generally accepted and was widely used in the metallurgy and pharmaceutical industries. Cooper and Eaton [10] working in the field of ceramic dry-pressing also came up with an expression which assumed three stages for the compaction process.

Although these various equations put forward are empirical, they have nonetheless proved very useful in quantitatively describing the compaction process and allowing comparative experiments to be carried out, albeit over a limited range of pressure and compaction speed. But none of these methods and other reported techniques [11], except very few [12–15], did consider the quantitative effect of the strain rate in the powder compaction process. Recently, however, Es-Saheb [16] investigated both the strain hardening and strain rate effects in some pharmaceutical powders under uniaxial compaction conditions by employing the general power law [17, 18] given as:

$$\sigma = B\varepsilon^n \dot{\varepsilon}^m \tag{2}$$

where σ is the axial stress (pressure) for an axial induced strain ε, n and m are the strain hardening and strain rate exponents respectively and B a constant.

To achieve better understanding of the compaction process mechanisms and to gain more accurate information as well as reliable quantitative measures of the powder properties, it is essential to evaluate and consider the values of strain hardening and strain rate exponents (n and m). This is particularly important for those powders most sensitive to strain rate and strain hardening properties, over wide range of pressures and compaction speeds.

In this paper the use of power-law for evaluating the compaction properties of four salt powders, namely: sodium chloride, potassium bromide, calcium phosphate, and copper sulfate is investigated. Also, the strain rate sensitivity and the strain hardening characteristics of these materials are evaluated. Furthermore, the strain hardening exponent n and the strain rate sensitivity index m, for these powders, over a wide range of strain rates (speeds) of 10^{-3} to 10^5 s^{-1} are determined.

MATERIALS

The investigation is carried out for the selected four salt powders, namely: sodium chloride (BDH Chemical Ltd., Germany), potassium bromide as well as copper sulfate pentahydrate (ICI Pharmaceutical Ltd., U.K.), and calcium phosphate (Albright and Wilson Ltd., U.K.) all in their normal laboratory form. The materials were used as received from the manufacturers. The true densities of these materials were determined using an air comparison pycnometer, Beckmann Model-930. Five determinations for each material were carried out and the mean value was calculated. The true densities found are 2170, 2750, 2295.5, and 2356 kg/m^3 for sodium chloride, potassium bromide, copper sulfate pentahydrate, and calcium phosphate respectively. For more details of these materials, including results of particle size analysis and electron scanning micrographs of the loose powders, reference [19] may be consulted.

EXPERIMENTAL METHODS

The tests cover low, medium, and high compression rates, a range of between 10^{-3} to 10^5 s^{-1}. Three different sets of apparatus and testing equipment were used to cover the different ranges of compaction rate. In all tests, high strength steel punches and dies were used to produce compact specimens of 10.0 mm diameter and 4.1 mm final height [14, 15, 20]. Typical characteristics plots were made for each powder in order to show the effect of strain hardening and strain rate on the powder behavior during axial compaction. These include: axial pressure *vs* axial strain rates plots, Heckel plots { $\ln[1/(1-D)]$ *vs* axial pressure} and strain hardening and strain rate exponents with axial strain rates.

Low Strain Rate (14×10^{-4} to 14 s^{-1})

The low strain rate compaction tests were carried out on a uniaxial compression machine whose crosshead speed was varied during the compression cycle through a computer controlled servo hydraulic system [15, 19, 20]. The compression tests were carried out at various constant compression rates, $\dot{\varepsilon}$, in accordance with the following equation:

$$\dot{\varepsilon} = d\varepsilon/dt = (1/H)dH/dt = V/H \tag{3}$$

assuming a uniform cross-sectional area of a cylindrical compact specimen. A constant rate was achieved by varying the cross-head speed, V, according to the current height of the specimen H.

The powders were pressed at constant compression rates of 14, 7, 1.4, 0.14, 0.014, and 0.0014 s^{-1}. During each test the axial pressure was monitored *via* load cells and the axial displacement of the punch by means of LVDTs.

Medium Strain Rate (10^2 to 10^3 s^{-1})

The medium strain rate compaction tests were carried out with the aid of a drop-hammer. The drop-hammer was originally built to provide the kinetic energy of a free falling tup mass for deforming various materials at velocities of up to 7 m/s. Essentially, the weight is dropped onto a punch which presses the powder specimen.

In this situation a constant compression rate is not possible because the impact velocity reduces to zero at the end of compression. However, an average or mean compression rate, $\bar{\dot{\varepsilon}}$ was used which is defined as the final degree of compaction, C, divided by the total duration time of the compaction process.

Typical speeds for the tup mass are in the range of 1.0 to 5.0 m/s and assuming a 50% final degree of compaction (*i.e.* $C = 0.5$) of a powder mass of initial height of 8.2 mm, compaction times between 5 to 50 ms were obtained. This produces an average compaction rate between 10^2 to 10^3 s^{-1}. In the tests carried out both the mass of the tup and the impact speed were varied to achieve specific compaction rates.

In each of the tests, the axial load from the load cell onto which the specimen was pressed and the axial displacement from a capacitance transducer were measured and acquired on storage oscilloscopes [19]. From these results, graphs showing the effect of compression rates and characteristic plots *e.g.* Heckel, axial pressure *vs* axial strain, *etc.* were made.

High Strain Rate (10^3 to 10^5 s^{-1})

In order to achieve higher compaction rate a new projectile launcher apparatus was built [15]. In this system, the load cell consists of a hardened steel die, the lower end of which fitted on to a long steel rod. This rod, which is instrumented with full bridge strain gauges along its length, replaced the lower punch in the conventional compaction arrangement and acted as a load cell for measuring the compaction load. The upper punch was arranged so that it could be rapidly driven into the die by the projectile. The change in volume (*i.e.* displacement) of the powder was measured by means of a variable capacitance unit which monitored the position of the punch [19].

Different levels of compaction and compaction speeds can be achieved by varying the pressure of the air gun and the use of different projectile types. The two types of bullets (projectiles) used were polythene bullets, turned from 10 mm diameter low density polythene rod, and, for higher compaction loads, lead bullets of about 16.0 g.

For each test, the outputs from the load cell and displacement transducers, as recorded on a time base by the oscilloscopes, were converted into applied pressure (stress) and degree of compaction (strain). Stress (pressure) *vs* strain curves and Heckel plots at the various strain rates were then constructed. The average strain rate, $\dot{\bar{\varepsilon}}$, calculated by dividing the total strain by the total compaction time and graphs of axial pressure *versus* strain rates are thus plotted covering the whole range of strain rates from 10^{-3} to 10^5 s^{-1}.

For each material three compression tests, at least, were carried out at each compression rate, and the mean values were calculated. The results and data analysis and manipulation for the three categories of strain rate experiments, low, medium, and high rates are presented below.

DATA MANIPULATION AND TREATMENT OF RESULTS

In this investigation, Equation (2) was used to analyze the relationship among the strain ε, the strain rate $\dot{\varepsilon}$ measured during compaction, and the applied pressure P (*i.e.* axial stress, σ). These quantities, as mentioned earlier, are calculated from the UV recorder plots, for low strain rate tests, and the oscilloscope traces, for medium and high strain rate tests. At selected points along the time scale, the deflections of the axial displacement transducers and load cells traces were measured. Having calibrated these transducers and load cells before, it was possible to convert these deflections into force (kN) and displacement (mm) respectively. Typical load–displacement curve for sodium chloride powder compacted at low speed (strain rate) is shown in Figure 1. Knowledge of the punches cross sectional areas, the initial compact height, and the elastic deformation of the compacting system (*i.e.* the machine rigidity), enable the force to be converted to axial pressure P (axial stress, σ), and the displacement to strain ε, and consequently to strain rate $\dot{\varepsilon}$.

However, to determine the strain hardening exponent n and strain rate sensitivity index m, using the power law, for each test the experimental compaction data obtained were manipulated in two states. These are:

1. The Determination of Strain Hardening Exponent, n

To determine the strain hardening exponent n for the powder, the power law given by Equation (2) is applied at each speed (*i.e.* strain rate $\dot{\varepsilon}$). However, to be able to employ this law, it is necessary to separate the effect of the strain (ε) and strain hardening from that of the strain rate ($\dot{\varepsilon}$). Thus, for the low strain rate tests (*i.e.* 10^{-3} to 10 s^{-1}) the issue is solved, because, as stated above, all materials were tested under constant compression rate conditions (*i.e.* at constant strain rate). Hence it was possible to separate strain rate effects. But, for medium and high strain rate tests, where the machines used for compaction engender strain rate effects, it was rather difficult to achieve the separation. Thus, as stated above, an average mean value for the strain rate ($\bar{\dot{\varepsilon}}$) is calculated for each test. This value, then, is considered to represent the constant compression rate for the test. Therefore, in this case, the power law given by Equation (2) is reduced to take the form:

$$\sigma = E\varepsilon^n \ , \tag{4}$$

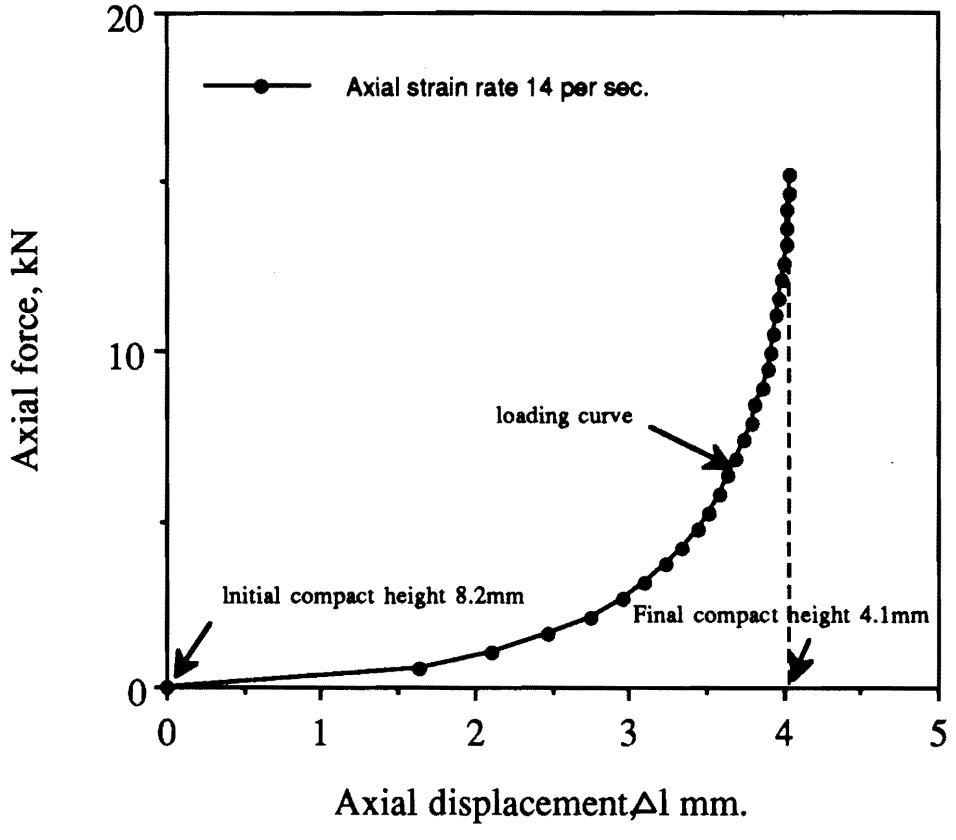

Figure 1. Typical Load–Displacement Curve for Sodium Chloride Powder Compacted at Low Strain Rate Range.

where σ is the axial stress (pressure), ε is the axial strain induced, and E is a constant. This constant actually presents the combined value of the terms B and $\dot{\varepsilon}^{\,m}$ given by Equation (2), where $\dot{\varepsilon}$ here is actually the constant strain rate value for the low strain rate tests and the average mean value $\bar{\dot{\varepsilon}}$ for the medium and high strain rate tests respectively. Thus, for each test, the axial pressure (stress σ) and the axial induced strain ε were calculated as mentioned earlier. These results, first, are plotted on log-log scales (see Figure 2), where the three distinct regions of the compaction curve (*i.e.* process) are clearly identified [18]. Actually, these regions present the well known stages of powder compaction [9, 19]. The initial mechanism involves particle rearrangement and packing down (*i.e.* region I), followed by elastic-plastic deformation and fragmentation (*i.e.* region II), and finally cold-working with or without particle ittrition (*i.e.* region III). Consequently, the experimental results over the third region (*i.e.* the region of prime concern) are, then, fitted with the best straight line, the slope of which represents the value of the strain hardening exponent, n, and the interpolation intercept of this line with the y-axis at unit strain represents the value of the constant E (*i.e.* the strength coefficient of the material). For each rate (*i.e.* speed) a mean curve, obtained from three compression tests, is taken as being representative and these curves for all rates tested are plotted on a common axis for each material. Typical example of this plot for sodium chloride powder, compacted at low strain rate range (*e.g.* at compression rate of 14 s^{-1}), is shown in Figure 2. The three compaction stages are displayed together with the best line fit of region III for this case, with a slope (*i.e.* n) equal to $\sim$ 3.7. While the variation of the strain hardening exponent n and the constant E with the strain rate for the powders tested are shown in Figures 3 and 4 respectively.

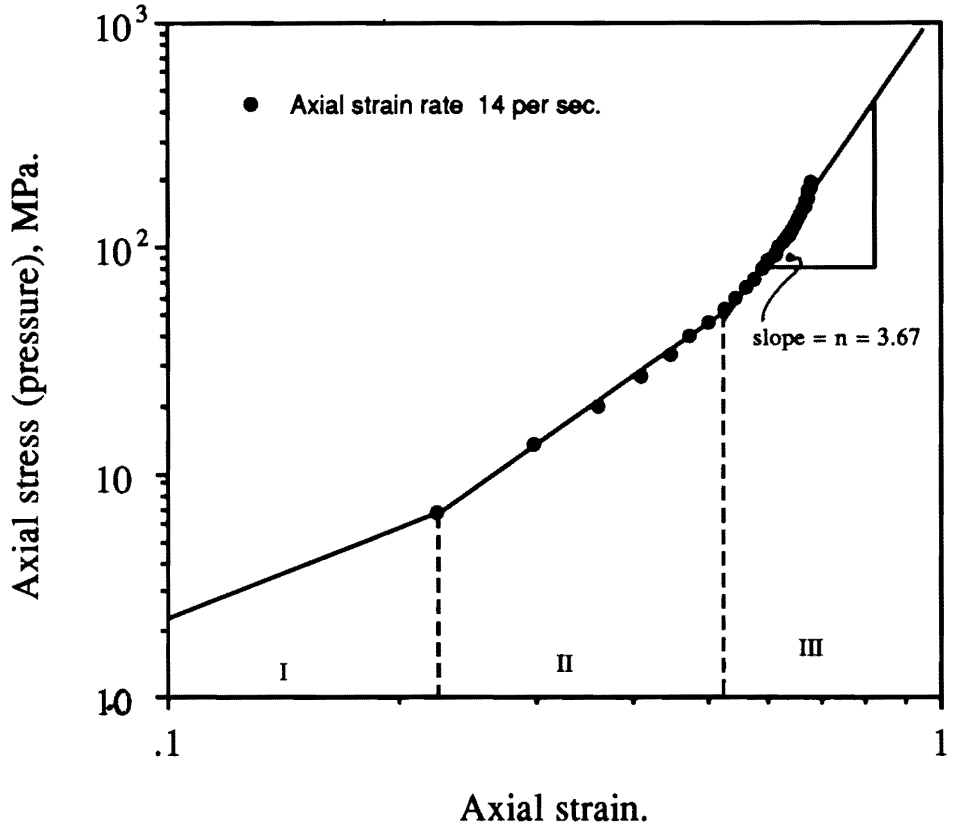

Figure 2. Typical Axial Pressure (σ) Axial Strain (ε) Plots for Sodium Chloride Powder Compacted at Low Strain Rate Range.

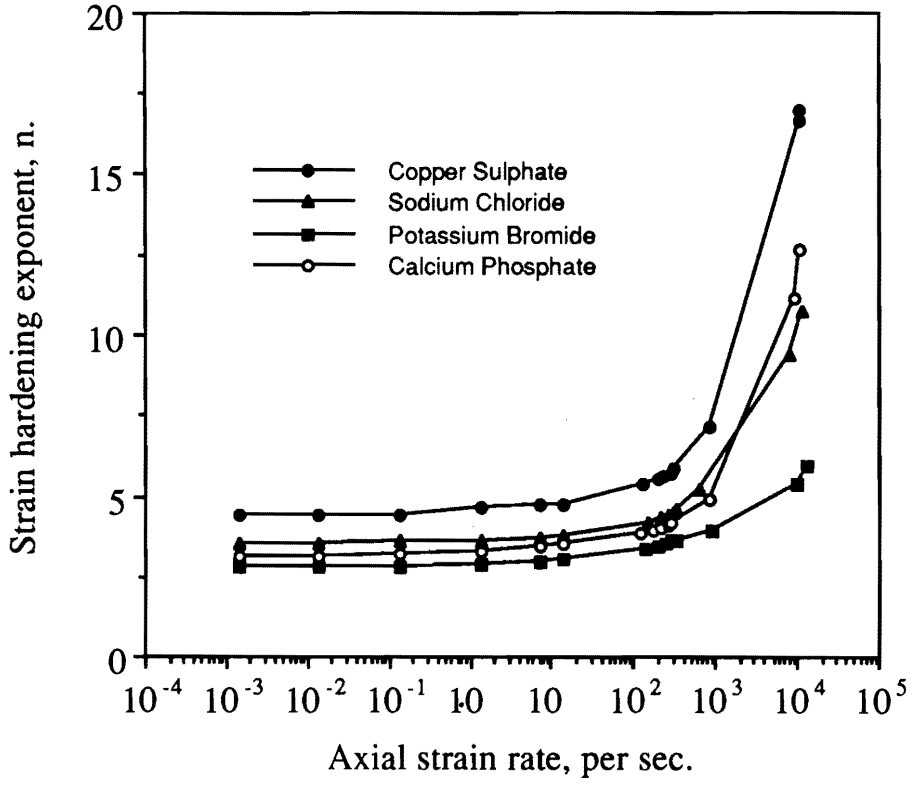

Figure 3. The Variation of the Strain Hardening Exponent (n) with the Axial Strain Rate ($\dot{\varepsilon}$).

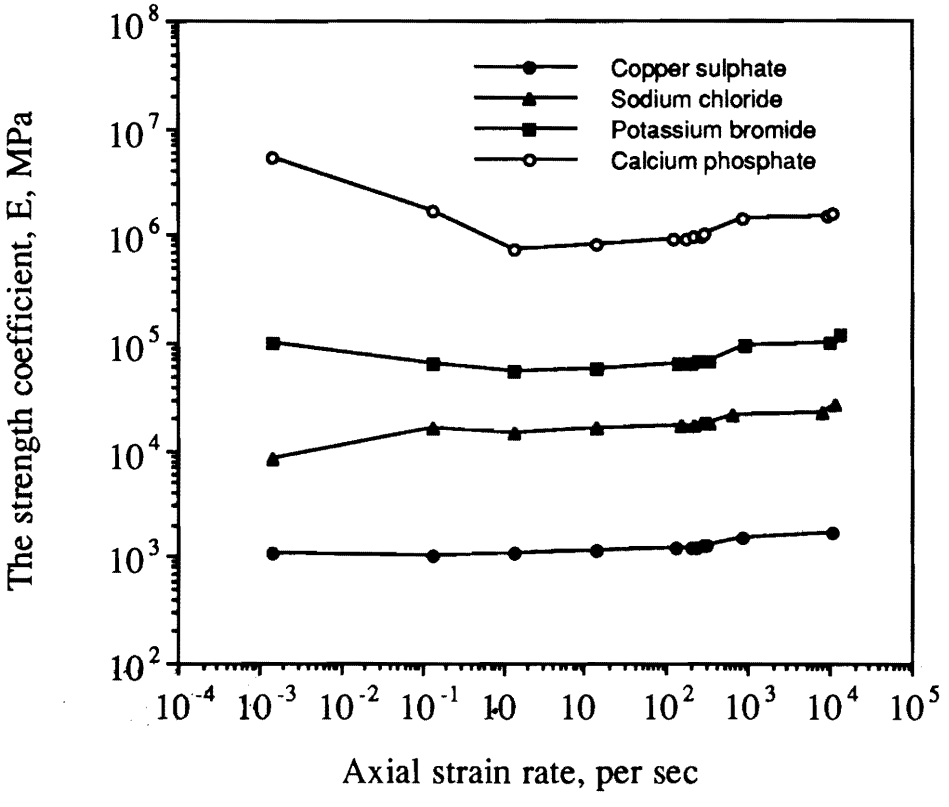

Figure 4. The Variation of the Stress Coefficient Constant E with the Axial Strain Rate ($\dot{\varepsilon}$).

2. The Determination of Strain Rate Exponent, m

After obtaining the mean values of the constant E and the strain hardening exponent n for each case, and taking these values to be constant at each strain rate (speed) condition. The power law is used once again to manipulate the data, to calculate the strain rate exponent m. Thus the power law could be reduced to take the form:

$$\bar{\sigma} = F \dot{\varepsilon}^{m} \tag{5}$$

where, in this case, F is a constant which incorporate the combined effect of the terms E and ε^n given by Equation (4), $\bar{\sigma}$ is the flow stress (pressure), $\dot{\varepsilon}$ is the strain rate, which is the constant compression rate for the slow tests and the average mean values ($\dot{\bar{\varepsilon}}$) for the medium and high rate tests respectively, and m is the strain rate exponent. But, to implement this equation the value of the flow stress has to be evaluated first for each test. However, to determine this value (*i.e.* the flow stress) for a powder it is very difficult. Because there is not a single distinct value which would describe the flow stress for the whole particles in a powder mass. Thus the mean yield pressure $1/K$ as determined by the Heckel Equation (1) is used to present reasonably the flow stress for the powder. Consequently, the values of the axial pressure P and the relative density D for the powders were calculated from the experimental data for each test. As described earlier, from the knowledge of the materials true density, the exact weight and compact current height, the relative density D for each test is calculated [15, 19]. Thus, it was possible to plot the Heckel curve for each test. However, for each rate (*i.e.* speed of compaction) a mean curve from three compression tests is taken as being representative, and these curves for all speeds tested are plotted on a common axis for each material. Then, from these Heckel plots, for each case the values of the constant K and its reciprocal (*i.e.* $1/K$, the mean yield pressure of the powder) are calculated. Typical examples of this plot for sodium chloride powder, compacted at low and medium strain rate ranges, are shown in Figure 5. The variation of the mean yield pressure $1/K$, (*i.e.* the flow stress, $\bar{\sigma}$), for the materials examined with the strain rate $\dot{\varepsilon}$ on log–log scales are shown in Figure 6, from which it was possible to obtain the average values of the strain rate exponent m for each material. Finally, the variations of the strain rate exponent m over the whole strain rate ranges for all the materials investigated are shown in Figure 7.

DISCUSSION

It is known that frictional forces among powder particles as well as between the powder and the die wall always oppose the transmission of the applied pressure in its vicinity. Also, this friction condition is always changing during the compaction process according to the particles shape, die surface condition, speed of compaction *etc.* Consequently this results in uneven stress distribution and hence non-uniform density throughout the compact [21]. Thus, the use of the terms stress and strain in this text means the average values, which correspond to the terms pressure and volume changes (*i.e.* density) usually used in describing the powder compaction.

From Figure 3 it is clear that, for all powders tested, as the speed of compaction increases the value of n (*i.e.* strain hardening exponent) increases in a non-linear manner. Meanwhile the value of the constant E is slightly linearly increased as shown in Figure 4. But, actually, the variation of E with strain rate is non-linear because of the logarithmic scales used. The small changes and scatter observed in the values of E, (obtained from the three tests carried out at each compaction condition for the various powders tested), could be due to the different starting initial conditions (*i.e.* initial powder density) as a result of the small weight differences in the initial amount of the powder being compacted in each case. This is strongly affected by the powder particles size and shape and their distributions as reported earlier. Also, in this investigation a constant volume compression condition is adopted (*i.e.* for all powders a 4.1 mm final compact height is used, which gives $\sim$ 95% final relative density). Consequently and on this basis the exact weight of each powder to achieve this percentage is calculated [15, 19]. Practically, it is found that the exact weights, of fine powders (*e.g.* calcium phosphate) can be achieved with accuracy of $\sim$ 1%, compared with $\sim$ 5% in the case of coarse powders (*e.g.* copper sulfate).

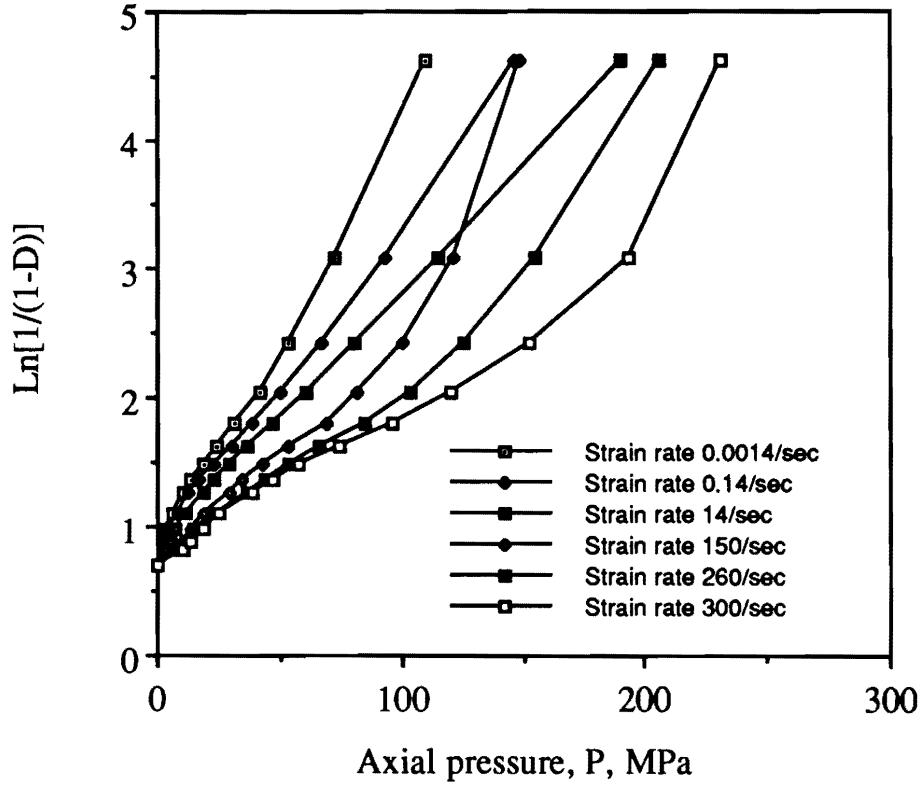

Figure 5. Typical Heckel Plots for Sodium Chloride Powder Compacted at Low and Medium Strain Rates.

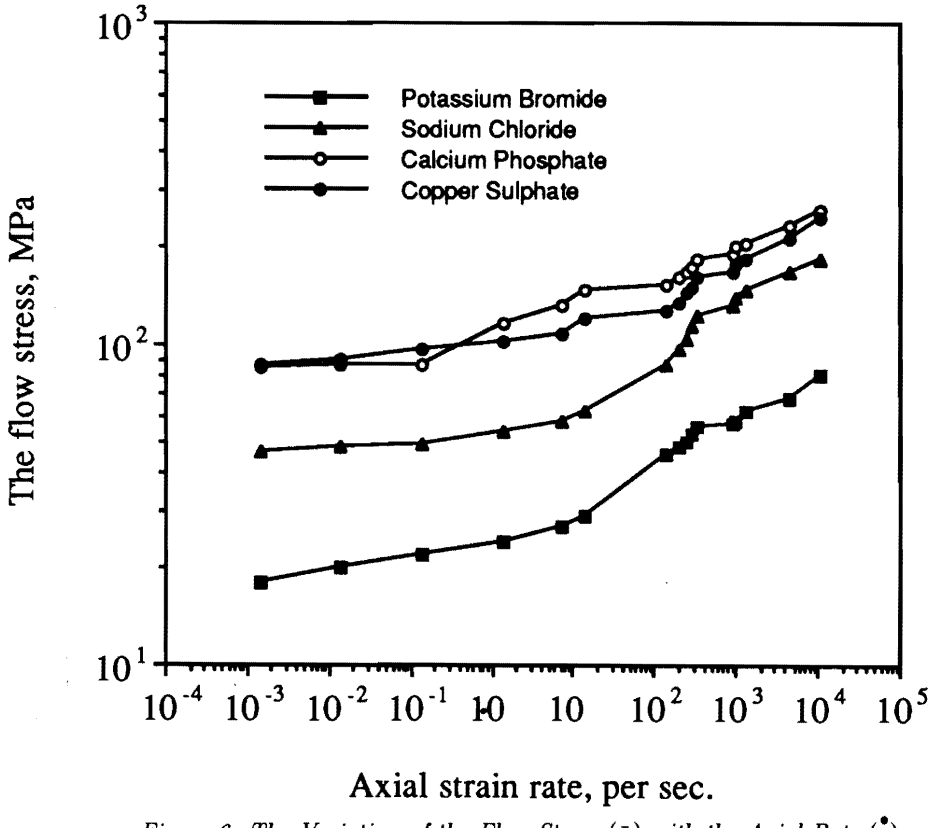

Figure 6. The Variation of the Flow Stress ($\bar{\sigma}$) with the Axial Rate ($\dot{\varepsilon}$).

In powder compaction, it is well known that the initial compaction conditions, particularly the initial density (*i.e.* packing is highly affected by the particles size and shape and their distributions) and the compaction speed have a vast effect on the success of the process and the final density of the compact [4, 8, 21, 22]. The compaction speed is, actually, affecting the various deformation and bonding mechanisms involved in the process. These in turn are manifested through the different types of dislocation and diffusion mechanisms involved in the process at each speed [12, 13, 15]. It is believed that at low speeds of compaction the powder is allowed enough time for the plastic deformation to take place through the well known dislocation mechanisms. At higher speeds the powder is observed to fracture and tends to become more brittle [13, 15] and the bonding of particles, in this case, is believed to be due to some form of diffusion mechanisms as a result of the short time durations involved in the process which does not allow the regular plastic deformation mechanism to take place [12–14]. Furthermore, it is established that the friction conditions, which are heavily affected by the powder surface conditions, powder particles size, and shape as well as their distributions and the compaction speed and powder mechanical properties [4, 11, 19], have a very significant effect on the initial compaction conditions and the subsequent deformation and bonding mechanisms involved in the process. These effects are reflected in the different values of the strain hardening exponent n and the strength constant E obtained for all powders and clearly shown in Figures 3 and 4 respectively. However, the particular effect of the compaction speed (*i.e.* strain rate) shown in the different values of m (*i.e.* strain rate exponent) and the flow stress will be discussed later.

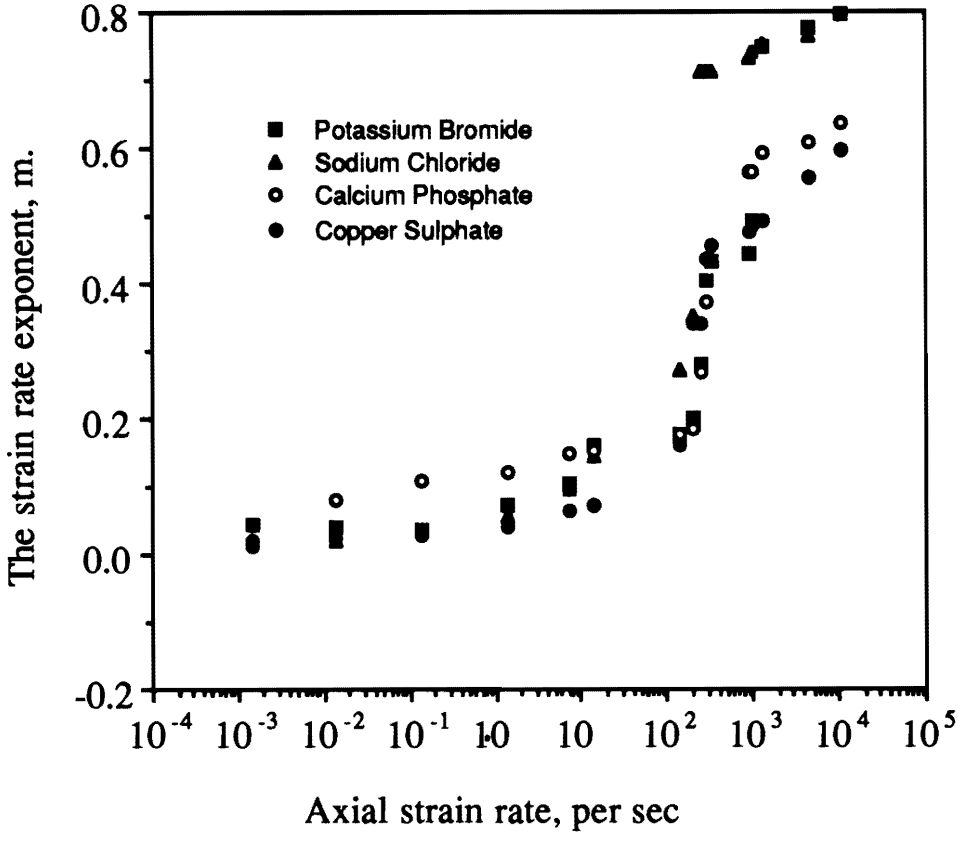

Figure 7. The Variation of the Strain Rate Exponent (m) *with the Axial Strain Rate* ($\dot{\varepsilon}$).

It is important to state that, the data presented in Figures 3 and 7 are calculated from tests carried out on three different 'rigs', (see the previous sections), to cover the whole tested ranges of strain rates. This dictates different compaction mechanisms to be operating during the compaction process at each range (*i.e.* at each rig). This is clearly shown in Figures 3 and 7, where each curve is noticed to consist of three portions, (each presenting a strain rate range), with n values tend to deviate clearly from one region to another as shown in Figure 3, (also see Figure 7 for m values). Also, it is important to remember that the data plotted in Figures 3 and 7 are on semi-log scales, which indicate non-linear variation of these parameters over the whole range including the first range where linear correlation is deceivingly displayed. This is also true in the case of parameter m shown in Figure 7.

It has been implied that the parameters E and n are material constants, and one cannot, for example, assume that the magnitude of these parameters is fixed for a material whose structure can be significantly altered by the speed and pressure of compaction. In effect, each chemical composition and condition of microstructure must be viewed as a different material as far as E and n are concerned. After all, E and n are the very parameters used to describe the work-hardening characteristics. Hence, the values of these constants are found to be indicative of the material properties and behavior including its morphology, deformation behavior (*i.e.* plastic and brittle) as well as the chemical structure. For example, the value of E is relatively higher for plastic "amorphous" material, and low speeds of compaction, while for brittle crystalline materials and relatively higher speeds, it becomes lower. This contrary to the change in values of n, *i.e.* higher values for crystalline brittle behaving materials and higher speeds, and lower values for plastic behaving materials and lower speeds. This can be clearly seen from the values of E and n, for the relatively plastic calcium phosphate where E is relatively high and n low, and the brittle and crystalline copper sulfate where E is relatively low and n is high. It must be considered, however, that the speed of compaction is always affecting the material behavior and hence the changes in the values of E and n.

Since these constants are believed to describe the effect of the initial material conditions, the material behavior and the deformation mechanisms, they could be used, in a similar manner to Heckel Equation constants, K and A, in characterizing the powder.

Furthermore, the significance of these constants, could be related to the 'capping' tendency in the various powders. It is noticed that when the value of E is high and n is low the capping tendency in certain materials is reduced (*e.g.* potassium bromide and sodium chloride powder), while if the value of E is low and n is high the capping tendency of the material is more likely, (*e.g.* copper sulfate powder). It is also noticed that, in almost all cases, the higher the value of $1/K$ (the mean yield pressure obtained from Heckel plot) the higher is the value of n and the lower is the value of E; while lower $1/K$ values coincide with lower n and higher E values. Consequently, the ascending order of the powders tested concerning its strain hardening properties, as shown in Figure 3, is potassium bromide, calcium phosphate, sodium chloride, and copper sulfate.

The combined effects of all deformation mechanisms involved in the process of compaction are very much affected by the speed of compaction, particularly the ductile and brittle behavior of the powder [13, 14], and consequently the form of the compaction curves. This clearly shown in the plots of Figure 5. However, at the higher strain rates and strains, non-linear behavior is noticed. This is believed to be due to the increasing brittle behavior of the various materials at this range of speeds and strains [17] as well as the cold working of the compact. This, however, differs from one powder to another depending on its mechanical properties and behavior under the various loading conditions. As expected all materials tested exhibit compression rate effects to some extent.

For all materials non-linearity is observed in the Heckel plots over the whole compaction pressure and speed ranges studied, see Figure 5. This indicates that all the materials examined do not deform exclusively by

plastic deformation mechanism, including the powders which are known to deform plastically such as potassium bromide and sodium chloride. It is noticed, also, as the speed of compaction increases the non-linearity of the plots increases. This indicates that fragmentation mechanism becomes increasingly dominant and the material tends to become more brittle [10], hence the increasing non-linearity of the Heckel plots and higher values of the mean yield pressure $1/K$. However, to determine the exact value of the mean yield pressure $1/K$, for each case, the incremental slope values of up to 30 points on the plot, particularly over the second stage of compaction (where the slope values change is very small) are calculated using a special computer software [15, 19]. Then the average slope value from these is calculated, the reciprocal of which is taken to be equal to $1/K$ value which considered to be the flow stress of the material. It is found that the descending order of the materials tested regarding its plastic deformation behavior as shown in Figures 5–7 is potassium bromide, sodium chloride, calcium phosphate, and copper sulfate. This, however, supports the earlier findings that the most brittle and crystalline materials are found to be more strain hardening during compaction (*i.e.* high values of n) with less plastic deformation and hence they show less sensitivity to strain rate (*i.e.* low values of m), such as copper sulfate powder.

As far as the compaction rate (speed) is concerned, Rees and Rue [22] found that with an increased contact time, *i.e.* slow speeds, they obtained a greater consolidation. But this is material dependent. A large change in consolidation with changing contact time is indicative of plastically deforming dominant material. This is in perfect agreement with our findings, which can be clearly seen from the values of $1/K$ obtained for the same powder at the various speeds of compaction and shown in Figure 6. It is noticed, also, that the variation of the mean yield pressure (*i.e.* the flow stress) with the axial strain rate starts almost linear at the very low speeds of compaction, where the plastic deformation mechanism is believed to be dominant and becomes increasingly non-linear as the speed increases. Rate effects are important, particularly, when one wishes to predict compaction loads at strain rates which may be as high as 10^5 s^{-1}, from data obtained in a laboratory compression test, in which the strain rates may be as low as 10^{-4} s^{-1}, the flow stress should be corrected unless m is very small. It is known that strain rate sensitivity is also, temperature dependent. Again it is important to mention here that, although the definition of m in the literature is, usually, based upon shear stress and strain rate, it is equivalent to the definition derived from Equation (5).

In the second stage of compaction differences between quasistatic and dynamic compaction behavior suggest that the yield strength of the powder must vary with the rate of compaction, see Figure 6. Numerous workers in solid mechanics have found that the flow stress of solids increases as the rate of deformation is increased. This, in fact, is in full agreement with our findings. The variation in flow stress with deformation rate, see Figure 6, is usually explained in terms of dislocation movement and interaction [23].

For the materials tested and many other metallic alloys [17] there is a minimum in m near room temperature and low strain rates, see Figure 7. However, as reported by Es-Saheb [16] for some composite powders, negative m-values are sometimes found, though this is not observed in the present investigation for any of the tested powders. In analogy with the observations in alloys [18] at low strain rates, solutes segregate to dislocations, (in the case of powders which are non homogeneous mixture by nature, *i.e.* a mixture of different sizes and shapes); this lowers their energy so that the forces required to move the dislocations are higher than those required for homogeneous materials. At increased rates, however, dislocations move faster than atoms can diffuse [17, 18], hence the drag is minimized. A very small rate sensitivity tends to localize flow in a narrow region which propagates along the compacted specimen as a band [16, 18], see Figure 7. This, also, could be attributable to the variation of the plastic deformation taking place within the powder mass during compaction as a result to the changing friction conditions effects. By localization of flow in a narrow band, the deforming material experiences a higher strain rate and therefore a lower flow stress. The higher values of rate sensitivity are attributed to the increased rate of thermally activated processes such as dislocation climb and grain boundary sliding [16–18].

From Figure 6 (which shows the dependence of flow stress, for all materials tested, upon strain rate) and Figure 7 (which shows the corresponding values of m as a function of strain rate), it is clear that, at the higher strain rates, m is typical of thermally activated slip. Meanwhile, at lower strain rates, deformation mechanisms other than slip prevail. Here there are two schools of thought [17, 18]. One maintains the deformation occurs primarily by diffusional creep with vacancies migrating from grain boundaries parallel to the compression axis to those normal to it. This diffusion causes the grains to contract in the compression direction and to elongate laterally. Whether diffusion is through the lattice or along grain-boundary paths, the strain rate should be proportional to the applied stress and inversely related to the grain size. If diffusion were the only mechanism, m would equal one (newtonian viscosity) but it is lowered because of the slip contribution to the overall strain. The other school attributes the high rate sensitivity to the role of grain-boundary sliding (shearing on grain boundaries). Although grain-boundary sliding alone would be viscous ($m = 1$), it must be accompanied by another mechanism to accommodate compatibility at triple points where the grains meet. Either slip or diffusion could serve as the accommodating mechanism. Both models explain the need for using very fine grain size materials (*e.g.* in the range of few microns) and low strain rates (*e.g.* as low as 10^{-4} s^{-1} to produce better compacts. But this practically present a dilemma, which necessitate a suitable compromise to be worked out for each specific application (*i.e.* for each powder size and speed of compaction to produce a certain product).

It is clear from Figure 7 also that the strain rate exponent m, for all the tested powders, varying in its value with the range of the strain rate resembling linear behavior at low speeds (where the glide mechanism is responsible for plastic deformation) and non-linear trend at higher rates (where the climb mechanism and diffusion are dominant). However, if the variation in m with the axial strain rate curves, shown in Figure 7 are approximated by straight lines, it is possible to identify three distinct main regions of variation. In the first and third regions (*i.e.* the low and high strain rate ranges), the variation in m with strain rate is small, though the compaction mechanisms are different (*i.e.* dislocation mechanism at low strain rate range and diffusion mechanisms at high strain rates), but it is slightly higher at the higher strain rate third region. Meanwhile in the second region (*i.e.* the medium strain rate range) the variation in m with strain rate is large. This could be attributed to the performance of the testing rigs employed over the three strain rate ranges investigated. Also, to the actual compaction behavior and strain rate mechanisms interaction for each material. This, also, indicates that different compaction and deformation mechanisms are dominant in each of these regions.

CONCLUSION

For all materials tested over the strain rate range of 10^{-3} to 10^{5} s^{-1} and the employment of the general power law for analysis it is concluded that:

1. The power law is shown to be sufficiently adequate for interpretation and characterization of the powder compaction process. The parameters E, n, and m derived from this law do incorporate and describe the numerous effects of compacted powders including the mechanical properties, deformation mechanisms, the morphology and the chemical structure as well as the speed of compaction (strain rate).
2. For all materials tested the variations of n, m, E, and σ with the strain rate $\dot{\varepsilon}$ are non linear.
3. All Heckel plots obtained are nonlinear which indicates that all the materials examined do not deform exclusively by plastic deformation mechanisms.
4. The more brittle crystalline materials (*e.g.* copper sulfate) show higher values of strain hardening exponent n and hence lower values of strain rate exponent m.
5. There is general tendency for all the powders tested to exhibit increased resistance to compaction with strain rate up to 10^{5} s^{-1}. The descending order of the powders tested regarding their strain rate sensitivity is potassium bromide, sodium chloride, calcium phosphate, and copper sulfate.

6. Both ductile and brittle behavior exist in the compaction process. At higher strain rates the brittle behavior dominates the process and compact capping becomes more prominent.
7. At low speeds, the plastic deformation mechanisms during compaction, are believed to be manifested by the dislocation mechanisms (slip, glide, climb, *etc.*), where adequate time is available. Meanwhile, at higher speeds (*i.e.* shorter time durations), some form of diffusion mechanisms tend to be the responsible.

REFERENCES

[1] W. H. Wallaston, "The Bakerian Lecture: On a Method of Rendering Platina Malleable", *Phil. Trans. of the Royal Society, Ser A,* **119** (1829), pp. 1-8.

[2] J. H. Shaxby and J. C. Evans, "On the Properties of Powders; The Variation of Pressure with Depth in Columns of Powders", *Trans. Faraday Soc.,* **19** (1923), pp. 60–72.

[3] E. E. Walker, "On the Properties of Powders; the Compressibility of Powders", *Trans. Faraday. Soc.,* **19** (1923), pp. 73–82.

[4] W. D. Jones, *Principles of Powder Metallurgy.* London: Edward Arnold, 1937.

[5] M. Y. Balshin, "Contribution to Theory of Metallo-Ceramic Processes Report IV. Contribution to Theory of Pressing Process". *Russian Translation Program RTS 6335, Vestnik Metalloprom,* **18(2)** (1938), pp. 124–137.

[6] K. Konopicky, "Parallelität der Gesetima big keiten in Keramik und Pulvermetallurgie", *Radex-Rundschau,* **3(7/8)** (1948), pp. 141–148.

[7] I. Shapiro and I. M. Kolthoff, "Studies on the Ageing of Precipitates and Co-precipitation; the Compressibility of Silver Bromide Powders", *J. Phys. Chem.,* **51** (1947), pp. 483–494.

[8] R. W. Heckel, "Density Pressure Relationships in Powder Compaction", *Trans. of Metallurgical Soc. of AIME,* **221** (1961), pp. 671–675.

[9] K. Kawakita and Y. Tsutsumi, "A Comparison of Equations for Powder Compaction", *Bull. Chem. Soc. Japan,* **39** (1966), pp. 1364–1368.

[10] A. R. Cooper Jr. and L. E. Eaton, "Compaction Behavior of Several Ceramic Powders", *J. Amer. Ceramic Soc.,* **45** (1962), pp. 1–97.

[11] I. Krycer, D. G. Pope, and J. A. Hersey, "The Interpretation of Powder Compaction Data — a Critical Review", *Drug Develop. and Inds. Pharmacy,* **8(3)** (1982), pp. 307–342.

[12] S. T. David and L. L. Augsburger, "Plastic Flow During Compression of Directly Compressible Fillers and its Effect on Tablet Strength", *J. Pharm. Sci.,* **66** (1977), p. 155.

[13] S. T. S. Al-Hassani and M. H. Es-Saheb, "Strain Rate Effects in Pharmaceutical Powders", *3rd Oxford Conf. on the High Strain Rate Properties of Materials, Oxford, U.K.,* April 9–12, 1984, p. 421.

[14] M. H. Es-Saheb, M. A. Sarumi, and S. T. S. Al-Hassani, "Compaction Rate Properties and Triaxial Stressing of Powders", *World Conf. on Powder Metallurgy (PM90), London, U.K.,* July 2–6, 1990, pp. 533–547.

[15] M. H. Es-Saheb, "Uniaxial Strain Rate Effects in Pharmaceutical Powders During Cold Compaction", *J. Mat. Sci.,* **27** (1992), pp. 4151-4159.

[16] M.H. Es-Saheb, "Powder Compaction Interpretation Using the Power Law", *J. Mat. Sci.,* **28** (1993), pp. 1269–1275.

[17] M. S. Soliman, "Breakdown of the Power-Law Creep in Class I A1–10 at %Zn Alloy", *J. Mat. Sci.,* **22** (1987), pp. 3529–3532.

[18] W. F. Hasford and R. M. Caddell, *Metal Forming Mechanics and Metallurgy.* Englewood Cliffs: Prentice Hall, 1983, pp. 49–102.

[19] M. H. H. Es-Saheb, "An Investigation into the Mechanics of Dynamic Compaction of Pharmaceutical Powders", *Ph.D. Thesis, University of Manchester, U.K.,* 1985.

[20] B. M. Hunter, D. G. Fisher, P. M. Pratt, and R. C. Rowe, "A High Speed Compression Simulator", *J. Pharm. Pharmac.,* **28** (1976), Suppl. 65P.

[21] D. S. El-Wakill, *Process and Design for Manufacturing.* Englewood Cliffs: Prentice Hall, 1989, pp. 228–230.

[22] J. E. Rees and P. J. Rue, "Time-Dependent Deformation of Some Direct Compression Excipients", *J. Pharm. Pharmac.,* **30(10)** (1978), pp. 601–607.

[23] J. D. Campbell, "Dynamic Plasticity: Macroscopic and Microscopic Aspects", *Mat. Sci. and Engineering,* **12** (1973), pp. 3–12.

Paper Received 28 September 1993; Revised 19 May 1994; Accepted 3 July 1995.